Clim Dyn (2012) 39:329–346
DOI 10.1007/s00382-011-1274-z

Predictability of the western North Pacific summer climate demonstrated by the coupled models of ENSEMBLES

Chaofan Li · Riyu Lu · Buwen Dong

Received: 4 March 2011 / Accepted: 12 December 2011 / Published online: 14 January 2012

Abstract The Asian monsoon system, including the western North Pacific (WNP), East Asian, and Indian monsoons, dominates the climate of the Asia-Indian Ocean-Pacific region, and plays a significant role in the global hydrological and energy cycles. The prediction of monsoons and associated climate features is a major challenge in seasonal time scale climate forecast. In this study, a comprehensive assessment of the interannual predictability of the WNP summer climate has been performed using the 1-month lead retrospective forecasts (hindcasts) of five state-of-the-art coupled models from ENSEMBLES for the period of 1960–2005. Spatial distribution of the temporal correlation coefficients shows that the interannual variation of precipitation is well predicted around the Maritime Continent and east of the Philippines. The high skills for the lower-tropospheric circulation and sea surface temperature (SST) spread over almost the whole WNP. These results indicate that the models in general successfully predict the interannual variation of the WNP summer climate. Two typical indices, the WNP summer precipitation index and the WNP lower-tropospheric circulation index (WNPMI), have been used to quantify the forecast skill. The correlation coefficient between five models' multi-model ensemble (MME) mean prediction and observations for the WNP summer precipitation index reaches 0.66 during 1979–2005 while it is 0.68 for the WNPMI during 1960–2005. The WNPMI-regressed anomalies of lower-tropospheric winds, SSTs and precipitation are similar between observations and MME. Further analysis suggests that prediction reliability of the WNP summer climate mainly arises from the atmosphere–ocean interaction over the tropical Indian and the tropical Pacific Ocean, implying that continuing improvement in the representation of the air–sea interaction over these regions in CGCMs is a key for long-lead seasonal forecast over the WNP and East Asia. On the other hand, the prediction of the WNP summer climate anomalies exhibits a remarkable spread resulted from uncertainty in initial conditions. The summer anomalies related to the prediction spread, including the lower-tropospheric circulation, SST and precipitation anomalies, show a Pacific-Japan or East Asia-Pacific pattern in the meridional direction over the WNP. Our further investigations suggest that the WNPMI prediction spread arises mainly from the internal dynamics in air–sea interaction over the WNP and Indian Ocean, since the local relationships among the anomalous SST, circulation, and precipitation associated with the spread are similar to those associated with the interannual variation of the WNPMI in both observations and MME. However, the magnitudes of these anomalies related to the spread are weaker, ranging from one third to a half of those anomalies associated with the interannual variation of the WNPMI in MME over the tropical Indian Ocean and subtropical WNP. These results further support that the improvement in the representation of the air–sea interaction over the tropical Indian Ocean and subtropical WNP in CGCMs is a key for reducing the prediction spread and for improving the long-lead seasonal forecast over the WNP and East Asia.

C. Li · R. Lu (✉)
State Key Laboratory of Numerical Modelling for Atmospheric Sciences and Geophysical Fluid Dynamics, Institute of Atmospheric Physics, Chinese Academy of Sciences, PO Box 9804, Beijing 100029, China
e-mail: lr@mail.iap.ac.cn

B. Dong
Department of Meteorology, National Centre for Atmospheric Science-Climate, University of Reading, Reading, UK

Keywords Western North Pacific · Coupled models · Seasonal forecast · ENSEMBLES · Summer climate · Prediction spread

1 Introduction

Summer climate over the western North Pacific (WNP), which is one of the most important components in the Asian monsoon system, has pronounced impacts on the climate over East Asia (e.g., Nitta 1987; Huang and Sun 1992; Lau et al. 2000; Lu 2001; Wang et al. 2001). The lower-tropospheric cyclonic/anticyclonic anomaly over the subtropical WNP, which is closely related to precipitation anomaly over the Philippine Sea and the zonal displacement of the WNP subtropical high, affects the summer rainfall over East Asia (Lu 2001; Wang et al. 2001). Thus, better understanding the predictability of the WNP summer anomalies is of central importance to the seasonal prediction of East Asian summer climate.

Fundamental discrepancies between the prediction of atmospheric general circulation models (AGCMs) and observations have been discussed in previous studies (e.g., Wang et al. 2004, 2005; Wu and Li 2008). In observations, the overall relationship between sea surface temperature (SST) and precipitation anomalies is negative over the WNP in summer (Wang et al. 2005; Wu et al. 2009). The AGCMs, however, when forced by observed or prescribed SST, yield positive SST-rainfall correlations and thus are unable to simulate correctly climate anomaly over the WNP. Accordingly, the forecast skills of AGCMs in predicting the WNP summer rainfall are considerably low (Wang et al. 2005; Kobayashi et al. 2005).

Since the beginning of the twenty-first century, the coupled ocean-atmosphere general circulation models (CGCMs) have been recognized as essential tools for seasonal prediction and climate diagnosis (Wang et al. 2008; Yang et al. 2008; Liang et al. 2009; Wang and Fan 2009; Yan et al. 2010; Rajeevan et al. 2011). Comparing with AGCMs, the CGCMs can better capture the atmospheric feedback on SST (Wu et al. 2006). Recently, Wang et al. (2008) investigated summer prediction of the leading modes on the large monsoon region of Asian-Australian monsoon with ten CGCMs for 1981–2001, and suggested that the models can successfully capture the first two dominant modes of interannual variability of the monsoon rainfall related to ENSO. Furthermore, Chowdary et al. (2009, 2010) focused on the predictability of the major leading modes of WNP summer climate following the mature phase of El Niño. Particularly, Chowdary et al. (2010) analysed the prediction results by 11 CGCMs from the previous EU project for seasonal predition (DEMETER, Palmer et al. 2004) and the APCC/CliPAS project (Wang et al. 2009) for the period 1980–2001, and pointed out that the coupled models are capable of well capturing the major modes of atmospheric variability over the WNP. They emphasized the contribution of the remote forcing in the tropical Indian Ocean and the local air–sea interactions after El Niño events in the preceding winter to the predictability of summer climate anomalies in the WNP. In addition, Lee et al. (2011) measured the forecast quality over the WNP and East Asian summer monsoon region with two coupled models, and suggested that the two models well predict the zonal wind anomalies in the lower troposphere during 1981–2006. They indicated that the correlation skill of the two model's ensemble reaches 0.75 with a January initial condition for the WNP summer monsoon index defined by Wang and Fan (1999), which is higher than that initiated from May due to some unknown reasons.

ENSEMBLES is an EU-funded integrated project that intends to develop an ensemble prediction system for climate change based on the principal state-of-the-art, high resolution global models developed in Europe. On one hand, the five leading European fully coupled models used in ENSEMBLES are well suited to assess current state of coupled predictability. Comparing with the previous prediction project (DEMETER), the models used in the ENSEMBLES have improved in many aspects including the increase in resolution, the better representation sub-grid scale physical processes, land, sea-ice and greenhouse gas boundary forcing and the more widespread use of assimilation for ocean initialization. On the other hand, while most previous studies focused on the summers after 1980, the 46-year hindcasts of 1960–2005 in ENSEMBLES offer an extended period for the investigation on the predictability of the WNP summer climate. Some previous studies have suggested that the teleconnection between the ENSO and tropical Indian Ocean and their influences on the WNP summer climate experience an interdecadal change since the late 1970s (e.g., Huang et al. 2010; Xie et al. 2010). The hindcasts for a longer period in the ENESMBLES would be helpful for better understanding statistically or physically the predictability of the WNP summer climate and its stationarity.

In this study, we attempt to provide an assessment on the predictability of the WNP summer climate, using retrospective forecasts (hindcasts) for the 46-year period of 1960–2005 obtained from the five leading European coupled models of ENSEMBLES. In particular, we investigate the atmospheric and oceanic variability associated with the prediction spread caused by different initial conditions, and discuss the sources of this atmospheric and oceanic variability.

The organization of this paper is as follows. Section 2 presents a description of models, hindcasts and datasets

used in this study. Section 3 provides a comprehensive assessment of the models forecasts on the WNP mean climate and interannual variability. Section 4 discusses the behavior of 45 integrations in the models and tries to identify the features of the spread for models prediction. Section 5 is devoted to a summary.

2 Models, hindcasts, and observational datasets

The models used in this study are the five fully coupled atmosphere-ocean-land prediction systems that come from a new seasonal-to-annual multi-model project named ENSEMBLES (van der Linden and Mitchell 2009), including the UK Met Office (UKMO), Météo-France (MF), the European Centre for Medium-Range Weather Forecasts (ECMWF), the Leibniz Institute of Marine Sciences at Kiel University (IFM-GEOMAR) and the Euro-Mediterranean Center for Climate Change (CMCC-INGV). Here, all models include major radiative forcing and have no flux adjustments. The atmosphere and ocean were initialized using realistic estimates of the observed states and each model was run from an ensemble of nine initial conditions. Table 1 presents a brief summary of main model components and their resolutions. Further details of the ENSEMBLES multi-model project and the models are referred to Doblas-Reyes et al. (2009, 2010) and van der Linden and Mitchell (2009).

The retrospective forecasts (hindcasts) of all five models have been performed for a 46-year period of 1960–2005. For each year, the seasonal forecasts are initialized on the 1st of May and are run for 7 months with 9 members for each model. The MME results are calculated through simple composite by applying equal weights to all five models.

The observed datasets used for model verification include monthly mean National Centers for Environmental Prediction/National Center for Atmospheric Research (NCEP/NCAR) reanalysis data (Kalnay et al. 1996) and NOAA Extended Reconstructed monthly mean SST V3 dataset (Smith and Reynolds 2004), with the time period from 1960 to 2005. The observational monthly precipitation data are obtained from Global Precipitation Climatology Project (GPCP) during 1979–2005 (Adler et al. 2003).

3 Assessment on the prediction of the WNP summer climate

3.1 Climatology

Figure 1 shows the climatology of JJA-mean (June, July and August) precipitation (1-month lead prediction) during 1979–2005 from ENSEMBLES models and GPCP. Comparing with GPCP, the five models and MME successfully capture the general features of summer rainfall with a pattern correlation ranging from 0.76 to 0.89. In observations, large rainfall mainly locates over the South China Sea (SCS), east of the Philippines, the East Asian Meiyu rainband, the Bay of Bengal, the tropical central-eastern Indian Ocean and tropical eastern Pacific Ocean (Fig. 1a). In the five models and MME, locations of the large climatological precipitation are well consistent with those shown in observations (Fig. 1b–g). However, all models predict a relatively stronger (2–4 mm day^{-1} stronger than observations) rainfall over east of the Philippines, especially for the MF and CMCC-INGV models.

For the lower-tropospheric winds, 1-month lead prediction from the ENSEMBLES models also captures well the major features of the climatological circulation in summer over the WNP. In observations, due to the existence of the subtropical anticyclone over the North Pacific, southwesterly from the Indian Ocean and easterly from the tropical Pacific Ocean join up around the Philippines and then change to strong southerly (Fig. 2a), and this southerly transports a large amount of water vapor into East Asia. Comparing with observations, the southwesterly from the Indian Ocean is stronger over the Philippines and the southerly from the SCS is weaker in models predictions and this is also true for the MME mean prediction (Fig. 2b–g). The weaker southerly in predictions is consistent with the weaker summer rainfall over the East Asian Meiyu rainband as less water vapor is transported to the continent during the rainy season (Fig. 1). The stronger convergence over the tropical WNP in models prediction than observations is also consistent with stronger predicted local rainfall (Fig. 1). These systematic biases over the SCS and WNP region mentioned above were also observed by many previous studies (e.g., Yang et al. 2008; Lee et al. 2010).

Table 1 Description of the five models used in this study

Partner	AGCM		OGCM	
	Model	Resolution	Model	Resolution
ECMWF	IFS CY31R1	T159/L62	HOPE	0.3°–1.4°/L29
IFM-GEOMAR	ECHAM5	T63/L31	MPI-OMI	1.5°/L40
MF	APPEGE4.6	T63	OPA8.2	2°/L31
UKMO	HadGEM2-A	N96/L38	HadGEM2-O	0.33°–1°/L20
CMCC-INGV	ECHAM5	T63/L19	OPA8.2	2°/L31

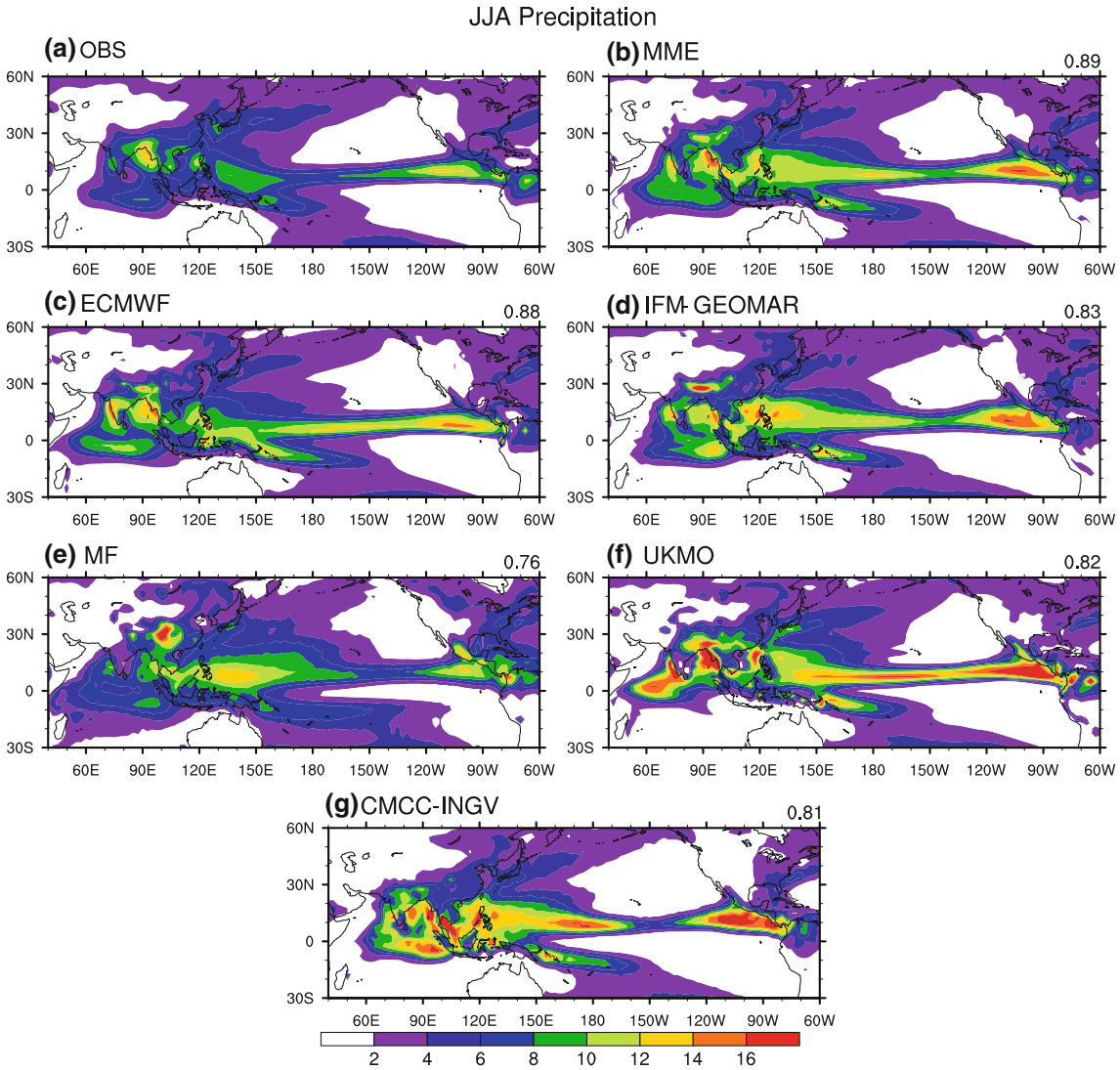

Fig. 1 The 1979–2005 climatology of JJA precipitation from **a** GPCP, **b** MME and the fives models of ENSEMBLES including **c** ECMWF, **d** IFM-GEOMAR, **e** MF, **f** UKMO, and **g** CMCC-INGV. Unit: mm day^{-1}. The *top right* values are the pattern correlation coefficients in the whole domain between the observations and models' prediction

Lee et al. (2010) found that considerable biases exist in both the amplitude and phase of the annual cycle and summer precipitation over there using 13 coupled models from DEMETER and APCC/CliPAS. These common biases in most of the coupled models indicate that correction of the inherent bias in the mean state is critical for improving the long-lead WNP summer prediction. Among the five models, ECMWF exhibits the best capability in simulating the climatological 850-hPa winds, in which the location and intensity of the winds are reasonably reproduced with high pattern correlations for both the zonal (0.96) and meridional (0.86) winds (Fig. 2c). In the IFM-GEOMAR and MF models, the ridge of the WNP anticyclone doesn't stretch westward enough and the axis of the ridge is not northeast-to-southwest extended as that in observations (Fig. 2d, e), which is consistent with the relatively stronger summer rainfall over the Philippine Sea in comparison with that over the Indian Ocean (Fig. 1d, e). Precipitation over these regions may affect the shape of the WNP anticyclone (Lu and Dong 2001;Rodwell and Hoskins 2001).

The climatological SSTs are also well reproduced for 1-month lead predictions by the ENSEMBLES models with a pattern correlation ranging from 0.95 to 0.97 (Fig. 3). In observations, the temperature reaches 29°C over the tropical western Pacific and the tropical Indian Ocean. These features are well captured by the ENSEMBLES models. However, the cold tongue over the east tropical Pacific predicted by ENSEMBLES stretches too westward than in observations, especially in the IFM-GEOMAR and CMCC-INGV models. This is associated

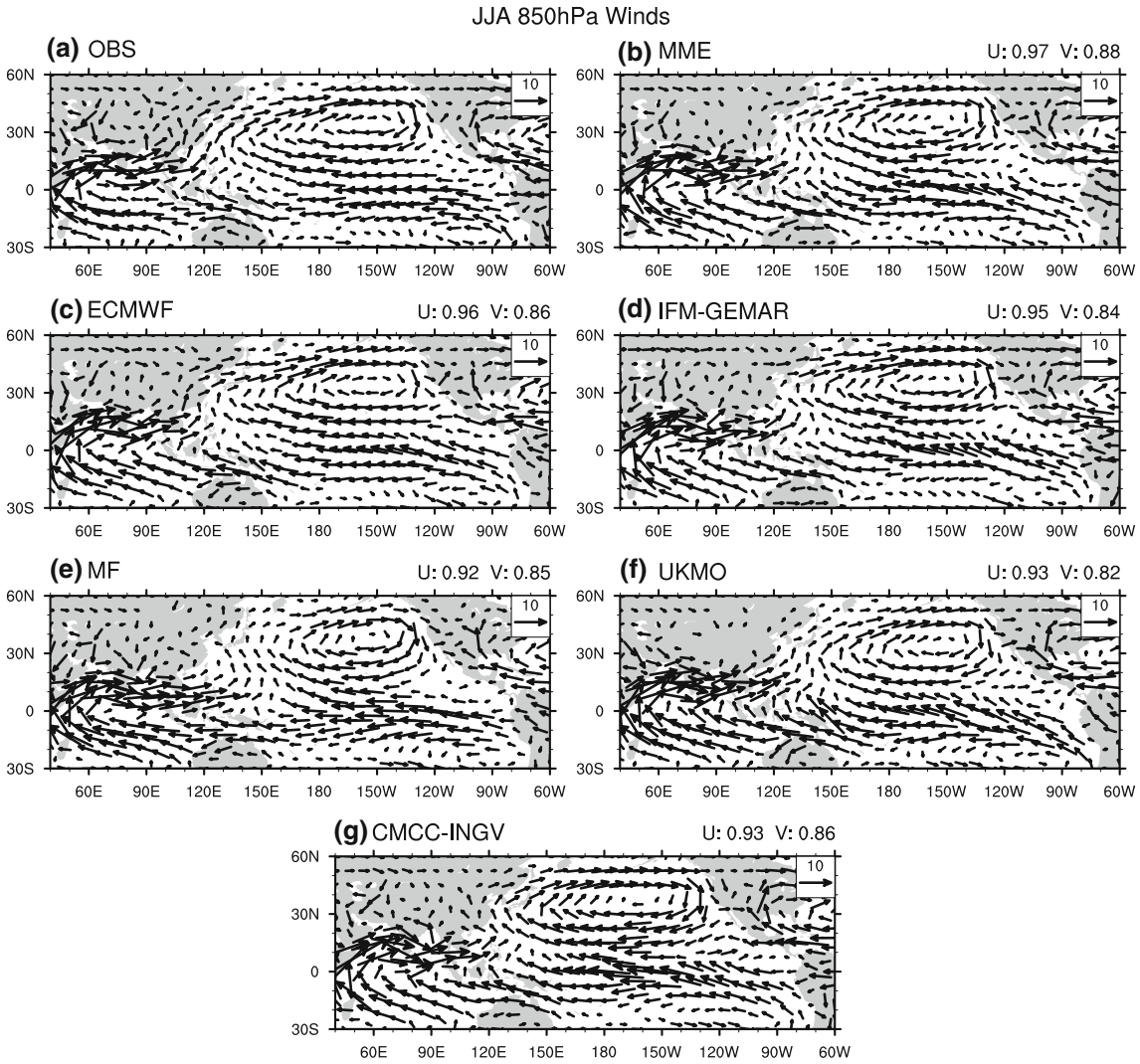

Fig. 2 Same as Fig. 1, but for the 850-hPa winds during 1960–2005 and the *top right* values are the pattern correlation coefficient of the zonal winds (U) and meridional winds (V), respectively. Unit for wind is in m s^{-1}

with stronger easterly trades in the tropical central and eastern Pacific and is responsible for the overestimation of precipitation over the WNP in the models predictions.

3.2 Prediction skills of interannual variability

In this subsection, the prediction skill of the interannual variability of the climate over the WNP will be assessed. To quantitatively measure the forecast skill, temporal correlation coefficient (TCC) calculated at each grid point is used. High TCC scores represent that the forecast has close relationship with observations.

The spatial patterns of TCC between models predictions and observations for precipitation during 1979–2005 are illustrated in Fig. 4. All models show a similar pattern of skill with the high skill regions being mainly over the tropical Pacific and the Maritime Continent. Figure 4 also indicates that all models, including the MME result, show good capability in predicting the interannual variation of precipitation over the Philippine Sea. Since anomalous positive (negative) precipitation over the Philippine Sea results in a cyclonic (anticyclonic) anomaly in the lower troposphere and this anomalous circulation further affects the East Asian summer climate (e.g., Nitta 1987; Lu 2001), a good performance of models on the Philippine Sea precipitation would favor a good prediction of the lower-tropospheric circulation anomalies in the WNP and East Asia. While high prediction skill mainly appears over the tropics, it declines rapidly to the north from the tropical region to the extratropical region. For instance, a poor prediction skill of the interannual variation of precipitation appears around east of Taiwan and over most of East Asian regions for individual models and for the MME mean. Understanding this poor prediction and

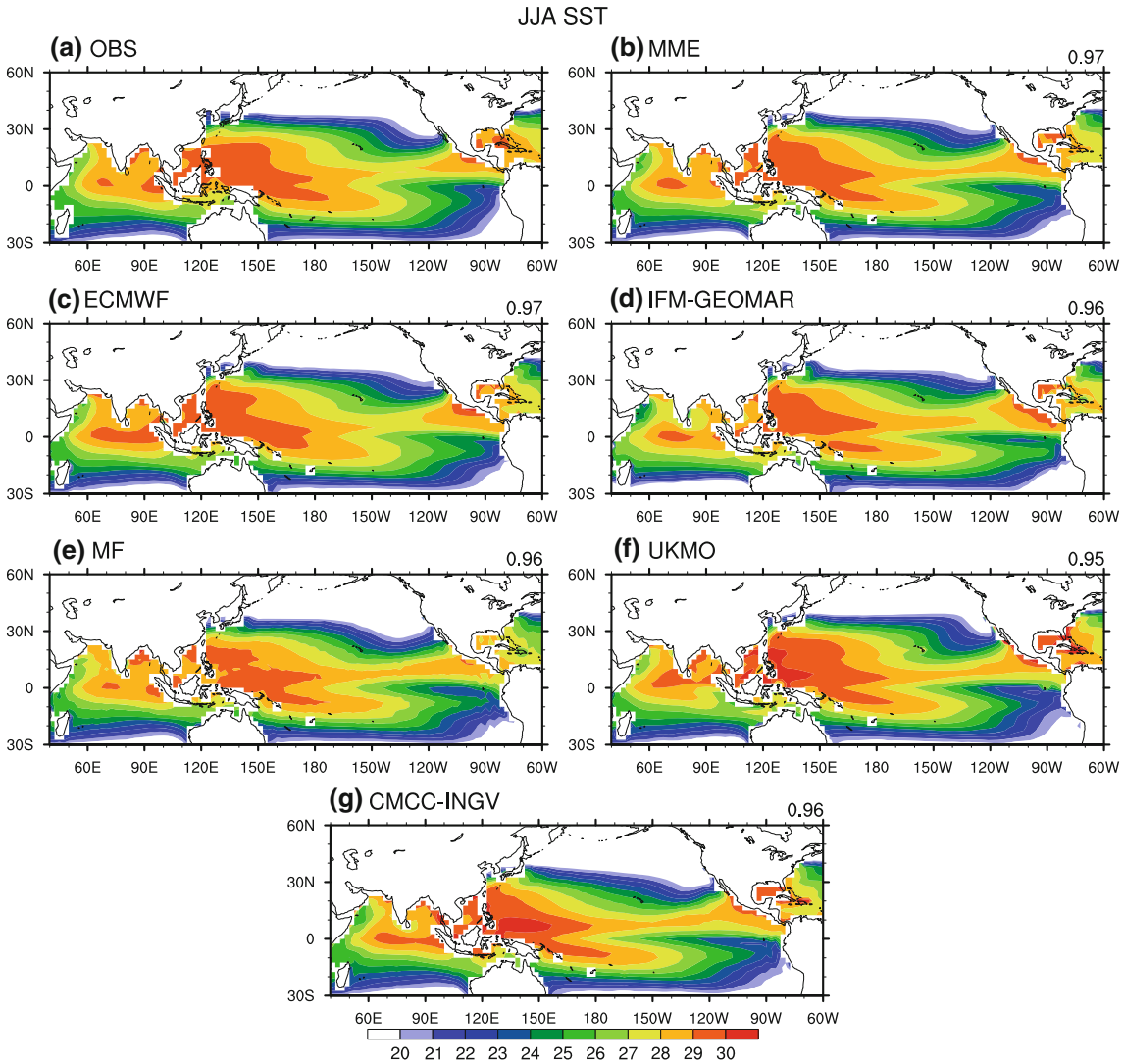

Fig. 3 Same as Fig. 1, but for SST. Unit: °C

improving seasonal forecasts of the East Asian summer rainfall in current CGCMs remain a major challenge. Figure 4 also shows that the Indian Ocean has a lower forecast skill where the correlation coefficients for all models do not exceed the significant confidence level of 0.05. This spatial distribution of the TCC for precipitation is similar to the previous results (Wang et al. 2009; Lee et al. 2011). In addition, negative TCC skills of precipitation are located over the north of the Maritime Continent. This might be related to the bias of ENSO-teleconnection in the models: the Niño 3 SST-related precipitation anomalies over the north of the Maritime Continent are negative in observations but positive in the models (not shown). The IFM-GEOMAR and CMCC-INGV show the strongest bias of the Niño 3 SST-related precipitation anomalies over the north of the Maritime Continent, being consistent with the most significantly negative TCC over this region (Fig. 4c, f).

Figure 5 shows the spatial patterns of the TCC for 850-hPa zonal wind. Comparing with skills of precipitation, high skill regions of the lower-tropospheric zonal wind extend to the north and cover the whole WNP region for all models, especially for the MME prediction. The highest skill appears over the tropical western Pacific Ocean, where the correlation coefficients are larger than 0.9. The good performance of the ENSEMBLES models on the lower-tropospheric circulation interannual variations over the WNP corresponds to high skills of predicted interannual variations in precipitation over the Philippine Sea (Fig. 4). In addition, prediction skills also exceed the 0.05 confidence level over the north Indian Ocean. However, some models show a deficiency over the SCS and east of Taiwan (Fig. 5b–f). For instance, the IFM-GEOMAR and CMCC-INGV models couldn't well reproduce the interannual variation of 850-hPa zonal wind over the northern SCS and the north Indian Ocean, and the UKMO

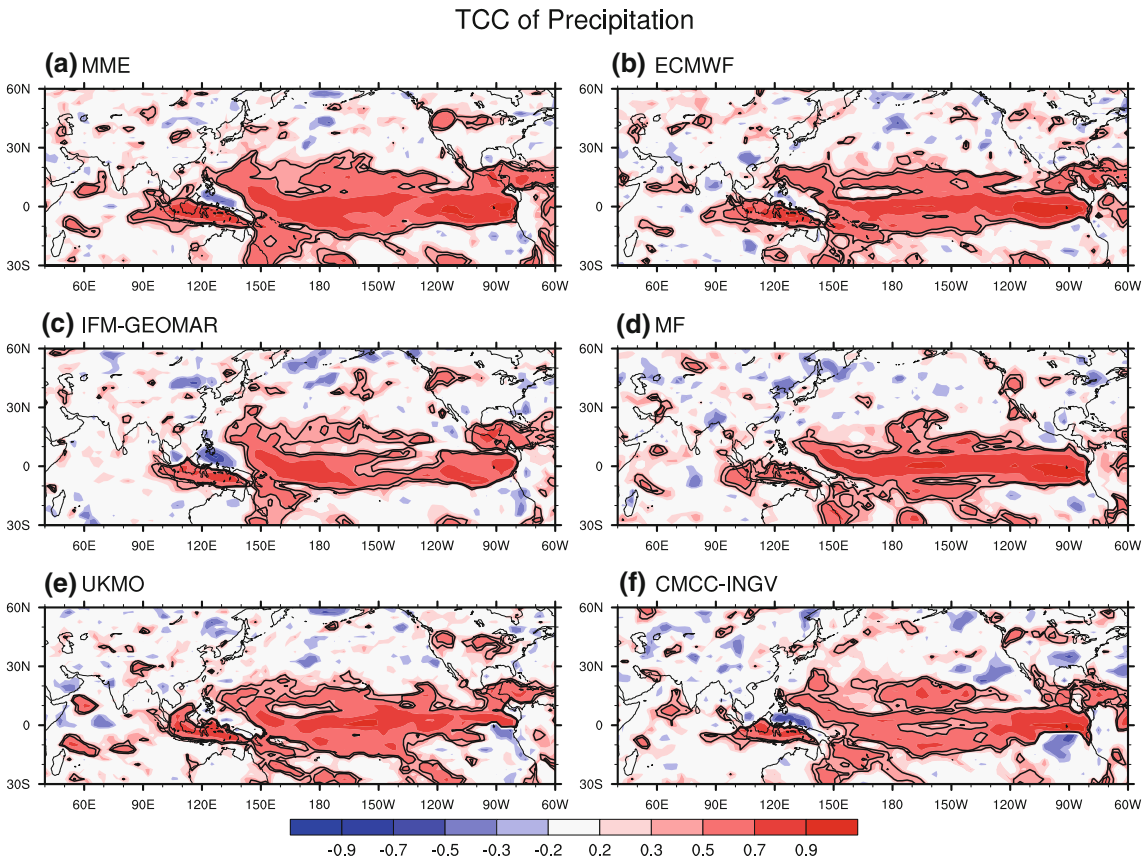

Fig. 4 Temporal correlation coefficients (TCC) for 1979–2005 JJA-mean precipitation between observation and **a** MME, **b** ECMWF, **c** IFM-GEOMAR, **d** MF, **e** UKMO, and **f** CMCC-INGV. The contours represent statistically significance of the correlation coefficients at 0.05 and 0.01 confidence levels, respectively

model exhibits relatively lower prediction skill over east of Taiwan.

Figure 6 illustrates the spatial distribution of the forecast skill of the interannual variability for SSTs. Relative to precipitation and lower-tropospheric zonal wind, SST is more predictable for its longer persistence and the TCC is greater than 0.7 in most tropical regions. Over the WNP, forecast skills decrease from the tropical warm pool region to the north. But the values still exceed the confidence level of 0.05 over most of the extratropical ocean. In MME, useful skills cover most oceanic regions while relatively lower skills appear over the equatorial Indian Ocean, the equatorial western Pacific, and the mid-high latitude WNP. Lower skills of the MME prediction in the equatorial Indian Ocean and the equatorial western Pacific mainly result from the low skills in the UKMO and CMCC-INGV models, and lower skills of the MME prediction in the mid-high latitude WNP result from the low skills in most models.

In general, considerable capability is demonstrated by the ENSEMBLES models on the summer climate prediction over the WNP. The high prediction skill for the lower-tropospheric circulation and SST almost covers the whole WNP region, and the precipitation is also well predicted over the Philippine Sea and Maritime Continent. These features suggest that current CGCMs demonstrate good performances in predicting the WNP summer anomalies.

3.3 Precipitation and lower-tropospheric circulation indices

Following Lu (2002), the WNP summer rainfall anomalies averaged over the region of (10°–20°N, 110°–160°E) is used to quantify the predication skill of interannual rainfall variations over the WNP. Figure 7 illustrates time series of the WNP JJA-mean rainfall anomalies during 1979–2005. The ENSEMBLES models successfully predict the negative rainfall anomalies in 1983 and 1998, though all models predict too strong negative anomalies in 1983 and one model predicts a near-normal rainfall anomaly in 1998. The rainfall anomalies are above normal or near normal since 1999 and this feature is well recalled by all models. However, all models couldn't well predict the positive rainfall anomalies in 1984: the MF and CMCC-INGV models show too weak positive anomalies and other three models produce weak negative anomalies.

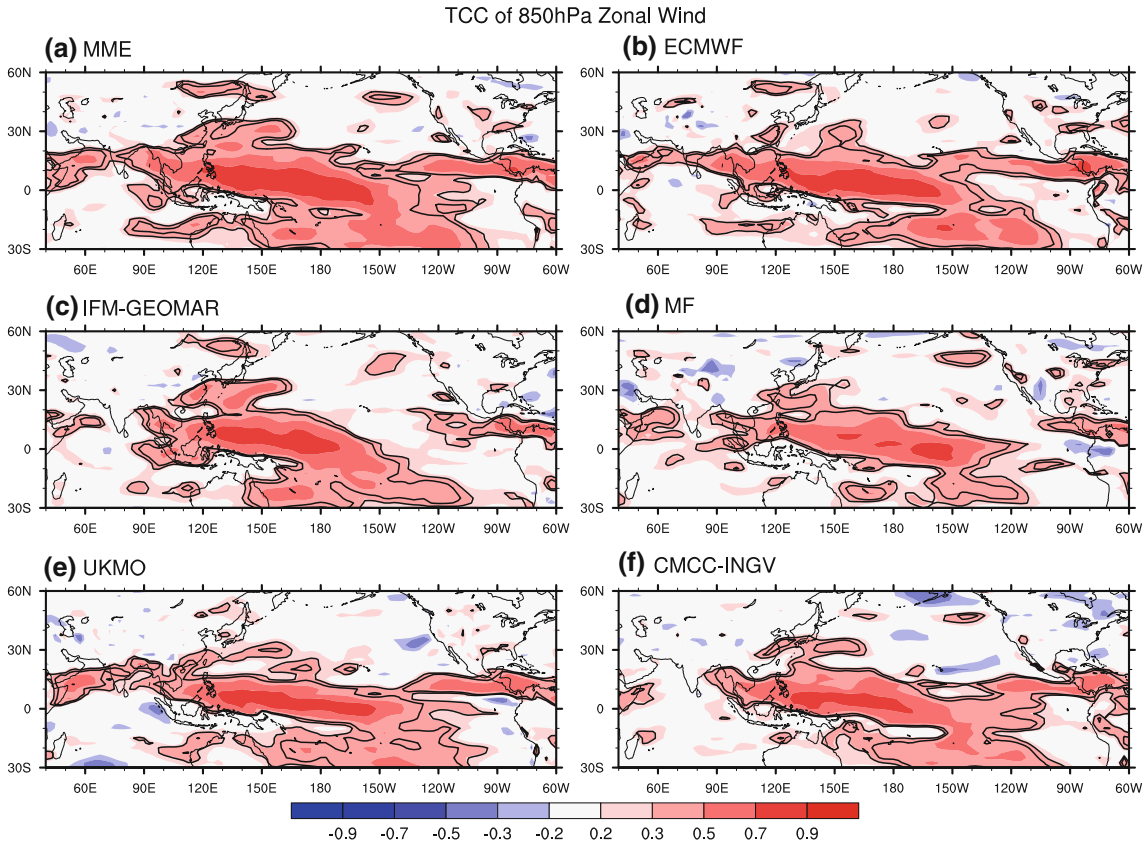

Fig. 5 Same as Fig. 4, but for the 850-hPa zonal wind during 1960–2005

Correlation coefficients of the rainfall anomalies between models and observations and the corresponding interannual standard deviation (SD) are shown in Table 2. The results show that the ENSEMBLES models demonstrate a reliable capability in predicting the interannual variation of the WNP summer precipitation. The MME and ECMWF exhibit the highest capability with the correlation coefficient between predictions and observations during 1979–2005 being 0.66. The MF model shows the lowest correlation coefficient of 0.46, but it still exceeds the 0.05 confidence level. In addition, SD of the WNP rainfall anomalies is also well predicted by the ENSEMBLES models. The SD predicted by MME is 1.09 mm day^{-1}, which is close to observed value (1.28 mm day^{-1}). The ECMWF, IFM-GEOMAR and MF models exhibit lower variability than observations, with SDs being 1.02, 0.93 and 0.76 mm day^{-1}, respectively; the UKMO and CMCC-INGV models show larger variability, with SDs being 1.41 and 1.31 mm day^{-1}, respectively.

Anomalous positive (negative) precipitation over the Philippine Sea leads to significant lower-tropospheric cyclonic (anticyclonic) anomalies over the WNP and thus is associated with zonal displacement of the North Pacific subtropical anticyclone (Lu 2001; Lu and Dong 2001). Following Wang and Fan (1999), a WNP monsoon index (WNPMI), defined as the difference of the 850-hPa zonal wind anomalies between (5°–15°N, 100°–130°E) and (20°–30°N, 110°–140°E), is used to quantify the interannual variation of the lower-tropospheric circulation and a positive index means an anomalous cyclonic circulation. The correlation coefficient between the WNPMI and WNP summer rainfall averaged over (10°–20°N, 110°–160°E) reaches 0.86 in observations during 1979–2005. Considering this close relationship, in the following we repeat the above analysis on the predicted rainfall averaged over (10°–20°N, 110°–160°E) through the WNPMI, for a longer period from 1960 to 2005.

The ENSEMBLES models reproduce the interannual variation of the WNPMI very well, as shown in Fig. 8 and Table 3. Firstly, the models predict the intensity of the WNPMI during most of years. For instance, negative anomalies in years of 1983, 1987, 1995 and 1998, which are corresponding to the El Niño decaying phase (Chou et al. 2003), are predicted rather well by all models. Similar to the WNP summer rainfall anomalies, the above-normal or near-normal anomalies of the WNPMI since 1999 are also well captured (Fig. 8). Secondly, the WNPMI reproduced by the models shows close relationships with that of observations. The minimum correlation coefficient between the forecasted and observed WNPMI reaches 0.54

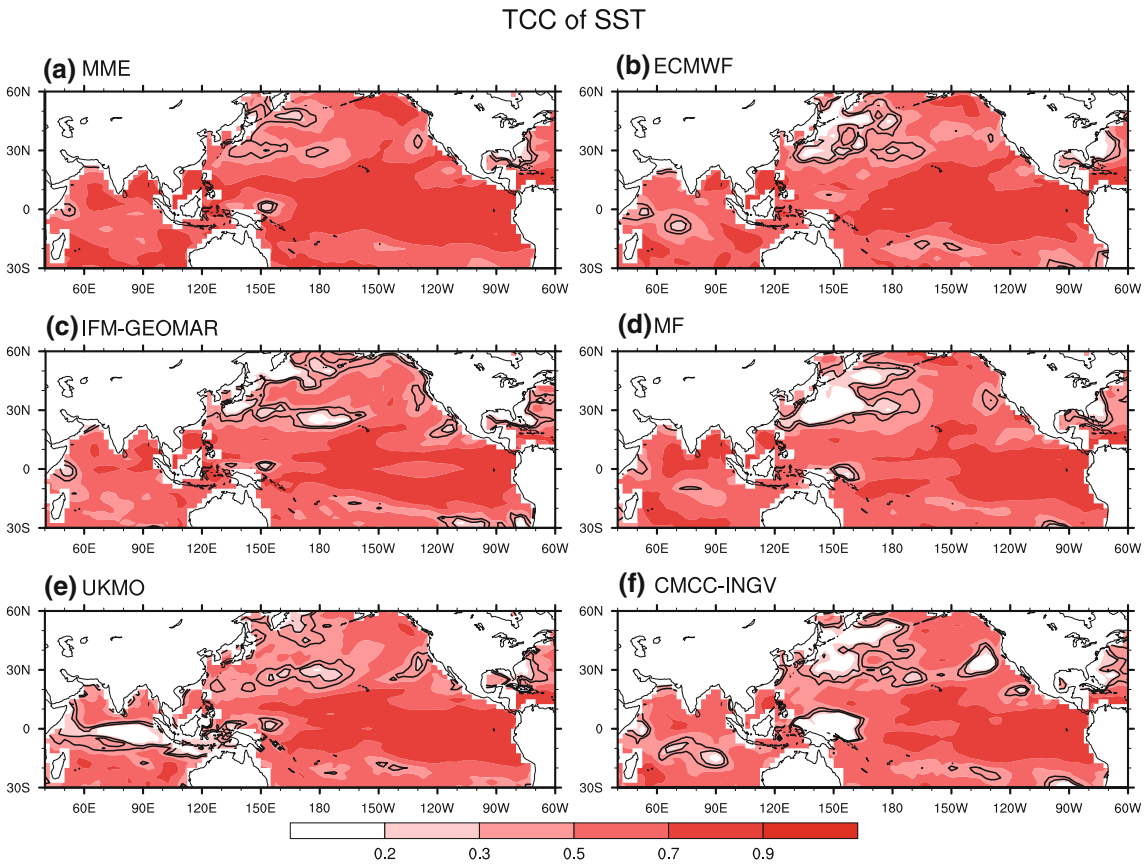

Fig. 6 Same as Fig. 5, but for SST

in the MF model during the 46 years and this correlation is statistically significant at 0.05 level (Table 3). The MME outperforms individual models and manifests its superiority with the correlation coefficient of 0.68 with the observed WNPMI. Similar analysis was carried out on the WNPMI by 12 state-of-the-art AGCMs from the CLIVAR C20C project in Zhou et al. (2009) and the result gave a correlation coefficient of 0.45 during 1950–2002 between the MME and observations. On the one hand, this suggests that AGCMs also show certain capability on the summer prediction of the WNP lower-tropospheric circulation. On the other hand, it implies that current AGCMs, even though they are forced by observed SST, couldn't predict the WNPMI as good as the fully coupled atmosphere-ocean models as described before in the introduction (Wang et al. 2004, 2005). In addition, the prediction skill of the WNPMI was also investigated by two coupled models' ensemble during the period of 1981–2006 and the correlation skill is around 0.6 for the May initiated data, as shown in Fig. 5b of Lee et al. (2011). In ENSEMBLES, the temporal correlation skill reaches 0.78 in the MME prediction during the similar time period of 1981–2005. Thirdly, interannual SD of the WNMPI is also well predicted by the coupled models. SD shown by the models is between 2.02 (MF) and

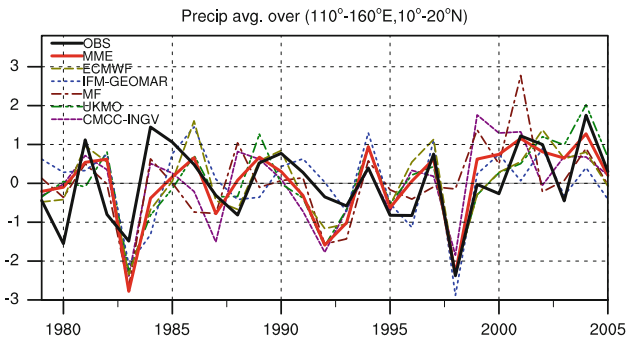

Fig. 7 Normalized time series of the JJA-mean precipitation anomalies averaged over the region of (110°–160°E, 10°–20°N) for the period of 1979–2005

2.38 (CMCC-INGV) m s^{-1}, which is similar to the observed SD (2.06 m s^{-1}). In addition, the close relationship between the WNPMI and the WNP precipitation index during 1979–2005 is also well captured by ENSEMBLES models. The correlation coefficient is 0.88 for the MME prediction.

Furthermore, the prediction skills of the two indices by the ENSEMBLES models are compared with those by the DEMETER models. The MME results during 1980–2001,

Table 2 Interannual variation of the WNP summer precipitation predicted by ENSEMBLES (the time series shown in Fig. 7), including the correlation coefficients between observations and models (left row) and the corresponding standard deviation (SD) (right row, Unit mm day^{-1})

WNP summer precip.	Corr. OBS	SD
OBS	–	1.28
MME	0.66	1.09
ECMWF	0.66	1.02
IFM-GEOMAR	0.53	0.93
MF	0.46	0.76
UKMO	0.58	1.41
CMCC-INGV	0.51	1.31

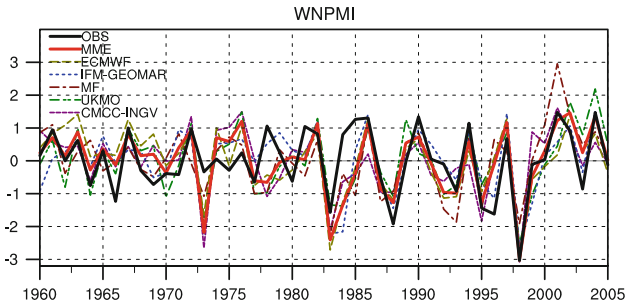

Fig. 8 Same as Fig. 7, but for the WNP summer monsoon index (WNPMI) during the period of 1960–2005

which is the hindcast period for the DEMETER models, are analyzed. On the one hand, the correlation coefficient of the WNP precipitation index between the MME prediction and observations is 0.63 in ENSEMBLES, and 0.56 in DEMETER. On the other hand, the correlation coefficients of the WNPMI are 0.77 and 0.79 in ENSEMBLES and DEMETER, respectively. The ENSEMBLES exhibits equivalent skills on the WNP climate anomalies with the DEMETER models. Furthermore, SDs of both the WNP precipitation index and the WNPMI predicted by DEMETER are smaller than those in observations, and they are better described by ENSEMBLES. The SDs of the WNP precipitation index (WNPMI) are 1.29 mm day^{-1} (2.58 m s^{-1}) in observations. They are 1.11 mm day^{-1} (2.53 m s^{-1}) in ENSEMBLES and 1.01 mm day^{-1} (2.22 m s^{-1}) in DEMETER MME results, respectively. The improvements of the prediction skills in ENSEMBLES are more significant over the Indian Ocean (not shown), which is similar to Rajeevan et al. (2011).

Our further examinations point out that the main features of lower-tropospheric circulation, SST and precipitation related to the interannual variation of the WNPMI in observations are well predicted by the models and they are illustrated in Fig. 9. In observations, associated with a positive WNPMI is a wave-like pattern of the lower-tropospheric circulation in the meridional direction, with an anomalous cyclone around 20°N over the WNP and an anomalous anticyclone around 35°N over East Asia. This distribution in the meridional direction over the WNP and East Asia is referred to as the Pacific-Japan (PJ) pattern (Nitta 1987) or East Asia–Pacific (EAP) pattern (Huang and Sun 1992). As Fig. 9a indicates, the westerly anomaly extending from the equatorial central Pacific to South Asia and the easterly anomaly over the subtropical WNP correspond to the southern and northern regions of the WNPMI, respectively. Concurrent with the anomalous lower-tropospheric circulation, SST anomalies exhibit a significant seesaw pattern in the meridional direction with warm anomalies of about 0.3°C over the mid-latitude WNP and cold anomalies of about 0.15°C over the WNP around east of Taiwan (Fig. 9c). In addition, there are negative SST anomalies of about 0.25°C in the north Indian Ocean and around the Philippines. The negative SST anomaly in the Indian Ocean is critical for the emergence and development of anomalous cyclone over the WNP, which was suggested by many previous studies (Terao and Kubota 2005; Yang et al. 2007; Li et al. 2008; Xie et al. 2009). In observations, precipitation anomalies related to a positive WNPMI are dominated by positive anomalies of about 0.6–0.8 mm day^{-1} in the Philippine Sea and negative anomalies of about 0.4 mm day^{-1} over East Asia (Fig. 9e). The positive precipitation anomalies in the Philippine Sea induce the cyclonic circulation anomalies in the lower troposphere over the WNP (e.g., Lu 2001; Huang 2004). The subtropical precipitation anomalies can also affect the circulation anomalies and favor for the maintenance of the meridional teleconnection over the WNP and East Asia (Lu and Lin 2009).

The major anomalies related to the WNPMI discussed above in observations are successfully captured by the models for the MME result (Fig. 9b, d, f). The anomalous cyclone associated with a positive WNPMI in the lower troposphere also locates around 20°N over the WNP (Fig. 9b). The negative SST anomalies over the Indian Ocean and the western tropical Pacific and positive precipitation anomalies over the Philippine Sea related to the WNPMI are also well described by the models (Fig. 9d, f). Although only the MME results are shown here, similar analyses have been performed on the results of each model, and each model shows similar spatial patterns of anomalies (not shown), suggesting consistency between the models. However, as the MME result indicates, the anticyclonic anomaly over the mid-latitude WNP and corresponding local positive SST anomalies are not well predicted by the models. The differences of the anomalies between MME and observations mainly appear in the extratropics, where

Table 3 Same as Table 2, but for the interannual variation of the WNPMI (the time series shown in Fig. 8) and Unit for SD is m s^{-1}

WNPMI	Corr. OBS	SD
OBS	–	2.06
MME	0.68	2.32
ECMWF	0.63	2.33
IFM-GEOMAR	0.67	2.57
MF	0.54	2.02
UKMO	0.58	2.32
CMCC-INGV	0.58	2.38

the atmospheric internal processes play an important role on the interannual variation (Lu et al. 2006). A positive SST anomaly appears over the equatorial central Pacific (Fig. 9d), which is slightly stronger than the observed one (Fig. 9c). This positive SST anomaly in the central Pacific appears in each model, particularly for the IFM-GEOMAR and UKMO (not shown). Both the observed and model results suggest that the SST anomalies in the equatorial central Pacific play a role in affecting the WNPMI variability. In addition, a significant positive SST anomaly locates in the subtropical central North Pacific in all the five models (not shown) and the MME prediction (Fig. 9d). This positive anomaly in the central Pacific and the negative SST anomaly in the subtropical WNP favor the maintenance of the WNP cyclonic anomaly through local air-sea interaction (Wang et al. 2000).

Despite the overall good skill of the ENSMBLES models on predicting the WNPMI, there are some deficiencies. The WNP summer lower-tropospheric circulation is not well predicted for some years as shown in Fig. 8. For example, the WNPMI in observations is near normal in 1973 while the anomalies predicted by all models exhibit a strong anticyclone over the WNP. This arises from the fact that the anticyclonic anomaly in observations locates over the east of the regions described by the WNPMI, but the anticyclonic anomaly predicted by the models extends too westward and covers the WNPMI regions (not shown). Another example is year 1984 when observations indicate a strong lower-tropospheric cyclonic anomaly over the WNP and an enhanced precipitation over the WNP, while models predictions do not capture these features. The prediction bias seems to be also related to ENSO phases (Chowdary et al. 2009) or significant bias in prediction of the meridional location of the East Asian upper-tropospheric westerly jet. The reasons for the poor prediction and the lying processes in these particular years need further investigations.

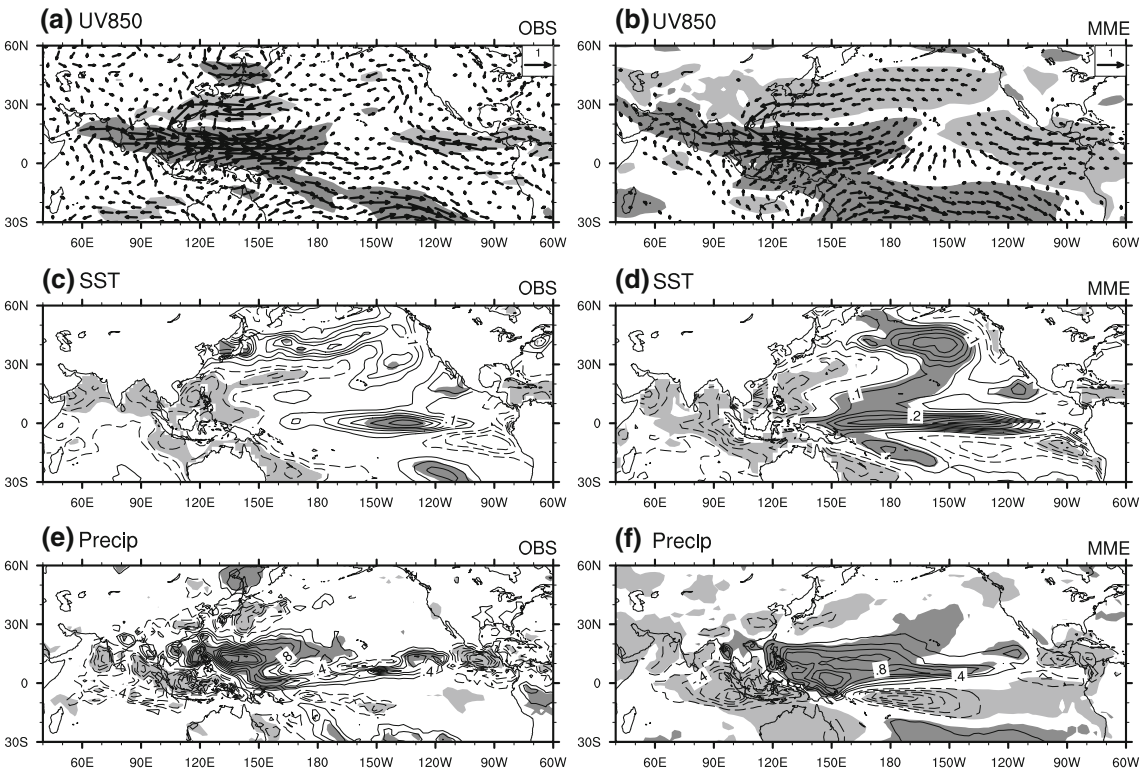

Fig. 9 Regression of the 850-hPa winds (*top*), SST (*middle*) and precipitation (*bottom*) anomalies onto the normalized WNPMI in observations (*left*) and MME (*right*), respectively. The *shading* indicates the regions where the anomalies are significant at 95% confidence level by using *t* test. The intervals of SST and precipitation anomalies are 0.05°C and 0.2 mm day^{-1}, respectively

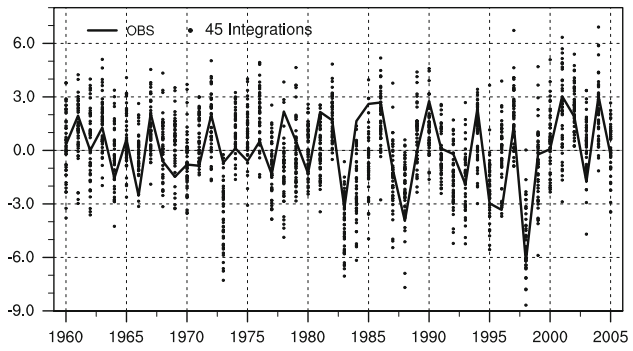

Fig. 10 WNPMI from observation (*line*) and 45 integrations (*dots*) of the models during 1960–2005. *Each dot* represents a predicted WNPMI in a particular year by individual models, and thus there are 45 dots for any a year

4 Spread of models predictions

An ensemble prediction with different initial conditions provides a way of distinguishing from the ensemble mean and the deviation from the ensemble mean, which is regarded as a measure of the noise and uncertainty lying in the initial conditions. In this section, we focus on the deviation from the ensemble mean and examine the features of the spread arising from different initial conditions. While each of the five models consists of 9 initial conditions, behavior of 45 integrations is described in this section.

Figure 10 shows the variation of the WNPMI from observations and 45 integrations of the models. There are two important points in this figure. Firstly, it suggests that current coupled models demonstrate considerable capability on the seasonal prediction of the WNP summer anomalies. In all the years except 1984, the observed WNPMI anomalies are within the ranges of predicted results of the 45 integrations. Secondly, the WNPMI described by the integrations of the models demonstrates significant spread. Standard deviation or variance of the 45 integrations is calculated year by year to quantitatively describe the intensity of the WNPMI's spread. The SD of the 45 integrations averaged over 1960–2005 is 1.62 m s^{-1}, which is two thirds of SD of the WNPMI interannual variation in MME (2.32 m s^{-1} as shown in Table 3).

Here, the WNPMI prediction of each integration $I(iy, im, \text{int})$ can be expressed as

$$I(iy, im, \text{int}) = [\bar{\bar{I}}(iy) - \bar{\bar{\bar{I}}}] + \bar{\bar{\bar{I}}} + [\bar{I}(im, iy) - \bar{\bar{I}}(iy)] + [I(iy, im, \text{int}) - \bar{I}(im, iy)],$$

where,iy, im and int are the corresponding year, model and integration for each prediction, respectively. Therefore, each integration of the model forecast can be recognized as the composite of three parts: $\bar{\bar{I}}(iy) - \bar{\bar{\bar{I}}}$ is the MME result of predicted WNPMI anomalies in a particular year; $\bar{I}(im, iy) - \bar{\bar{I}}(iy)$is the model-to-model deviation; $I(iy, im, \text{int}) - \bar{I}(im, iy)$is the noise caused by internal atmosphere-ocean coupling triggered by different initial conditions. The MME prediction results have been shown in Figs. 4, 5, 6, 7, 8, and 9. The other two components, including the deviation from MME arising from different models and noise arising from different initial conditions for a particular model, lead to the prediction spread and constrain the accuracy of seasonal prediction.

For the spread of the WNPMI shown in Fig. 10, the total variance of the 45 integrations averaged from 1960 to 2005 is 2.63 m^2 s^{-2}. Among it, the variances caused by the model-to-model deviation and different initial conditions, averaged over 1960–2005, are 0.79 and 1.84 m^2 s^{-2}, respectively. Thus, the spread caused by different initial conditions explains about 70% of total variance of the 45 integrations, much stronger than that caused by the model-to-model deviation. This indicates that the prediction spread of the WNPMI is mainly caused by the slight differences in the initial states of the atmosphere and ocean. The model-to-model deviation, on the other hand, plays a secondary role in causing the WNPMI prediction spread, which can be also confirmed by the fact that the observed WNPMI anomalies are within the ranges of predicted results of the 9 integrations by any a particular model in almost all the years (not shown).

Hence, in the following, we focus on the features of the circulation, precipitation and SST anomalies associated with the spread caused by different initial conditions. In order to examine the consistency and inconsistency between the models, the spread-associated features for each model are presented. The deviation between integrations of a model and this model's ensemble mean, that is, $I(iy, im, \text{int}) - \bar{I}(im, iy)$, is used to describe the spread. The sample size of the WNPMI spread for each model is 414 (9×46), and this spread index is normalized before regression. Features of the atmospheric circulation, SST, and precipitation spread in each model are analyzed through regression onto the spread of the WNPMI prediction.

Figure 11 shows the spread of the 850-hPa wind anomalies regressed onto the normalized WNPMI spread for each model. To facilitate the comparison with the observed and MME results shown in Fig. 9, the arithmetic average of the five models' results is also shown as Fig. 11f. Corresponding to a positive WNPMI of prediction spread in each model, there is a wave-like pattern with a cyclonic anomaly over the subtropical WNP and an anticyclonic anomaly over the mid-latitude WNP, for all models (Fig. 11a–e). Associated with the cyclonic anomaly over the subtropical WNP, a significant westerly anomaly appears over a broad region extending from the north

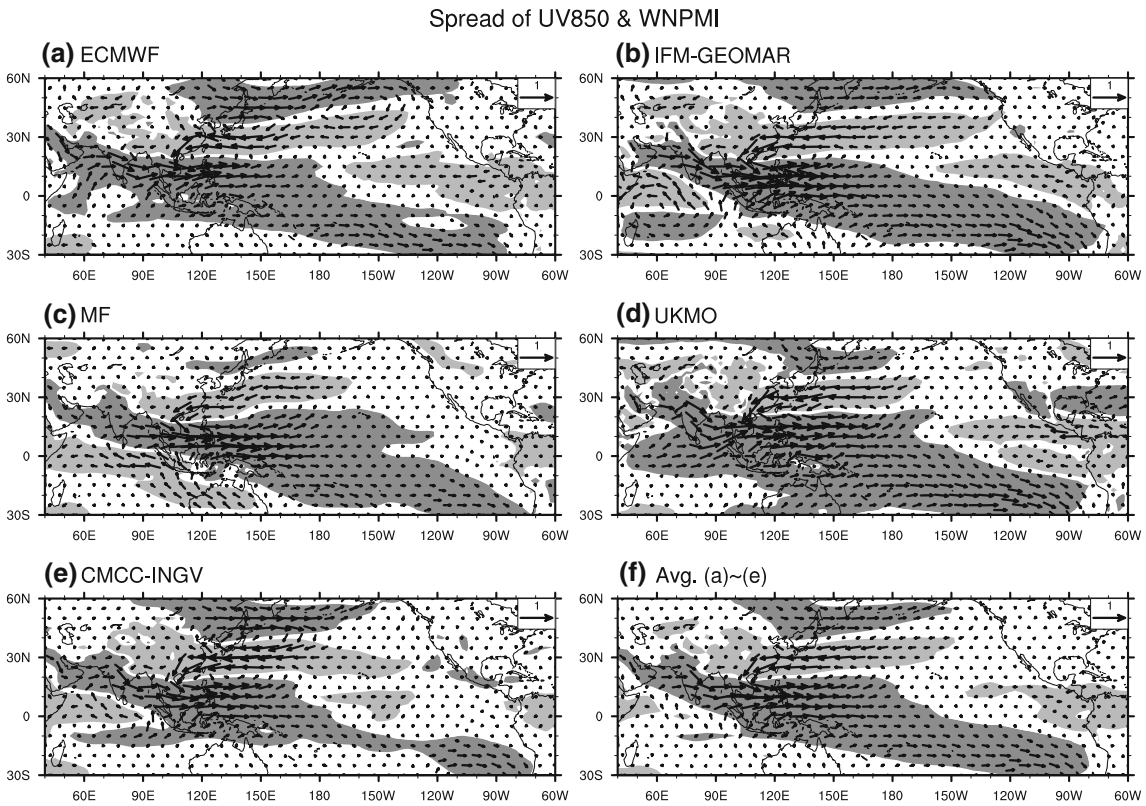

Fig. 11 Spread of 850-hPa wind anomalies regressed onto the normalized prediction spread of the WNPMI from different integrations of the five models **a** ECMWF, **b** IFM-GEOMAR, **c** MF, **d** UKMO, and **e** CMCC-INGV. The anomalies shown in **f** are the arithmetic averages over **a**–**e**. The WNPMI prediction spread has been normalized before regression. The *shading* indicates the regions where the anomalies of 850-hPa zonal wind are significant at 95% confidence level by using *t* test. Unit: m s^{-1}

Indian Ocean southeastward to tropical eastern South Pacific. These features of lower-tropospheric circulation anomalies are most clearly shown in Fig. 11f, and they show a spatial distribution similar to the WNPMI-regressed patterns in observations and MME (Fig. 9a, b). The five models illustrate well consistency with each other on these features of lower-tropospheric circulation anomalies. There is a westerly anomaly over the mid-latitude WNP associated with the prediction spread for all models (Fig. 11a–e), which appears in observations (Fig. 9a) but not in the MME prediction (Fig. 9b).

Figure 12 shows the spread of SST anomalies regressed onto the normalized WNPMI spread. SST anomalies associated with the spread are dominated by a seesaw pattern with cold anomalies (0.10–0.15°C) over the tropical/subtropical WNP and warm anomalies (0.10–0.15°C) in the mid-latitude WNP (Fig. 12). These features are evident for all models except the MF (Fig. 12a–e) and are therefore true for the mean pattern (Fig. 12f). The SST anomalies in the model MF are confined in the tropical region around the Maritime Continent (Fig. 12c). Negative SST anomalies appear over the north Indian Ocean for most models, but they are weak. Significant differences among the models are found over the tropics. There are strong positive SST anomalies in the equatorial Pacific for the model IFM-GEOMAR (Fig. 12b), which contributes to the weak positive SST anomalies for the averaged results (Fig. 12f), but there are no appreciable SST anomalies in the ECMWF, MF and CMCC-INGV.

The mean SST pattern associated with the spread of the WNPMI (Fig. 12f) shows some characteristics that are different from those associated with the interannual variability of the WNPMI for the MME prediction (Fig. 9d). These differences are summarized in Table 4. Over the north Indian Ocean (0°–25°N, 40°–100°E), the averaged SST anomaly in observations and MME is about −0.1°C, while it is only −0.028°C related to the spread. The magnitude of cold SST anomalies over the WNP associated with the spread (−0.076°C) is weaker than that associated with the WNPMI interannual variability for observations (−0.097°C) and the MME (−0.092°C) (Figs. 9, 12; Table 4). Differences between the MME and spread also appear over the mid-latitude WNP, where the averaged SST anomaly in the MME is 0.016°C and it is 0.062°C in the spread result (Table 4). In summary, the SST anomalies associated with the WNPMI interannual variability in the MME resemble well those in observations in the tropics, while the SST anomalies associated with the prediction

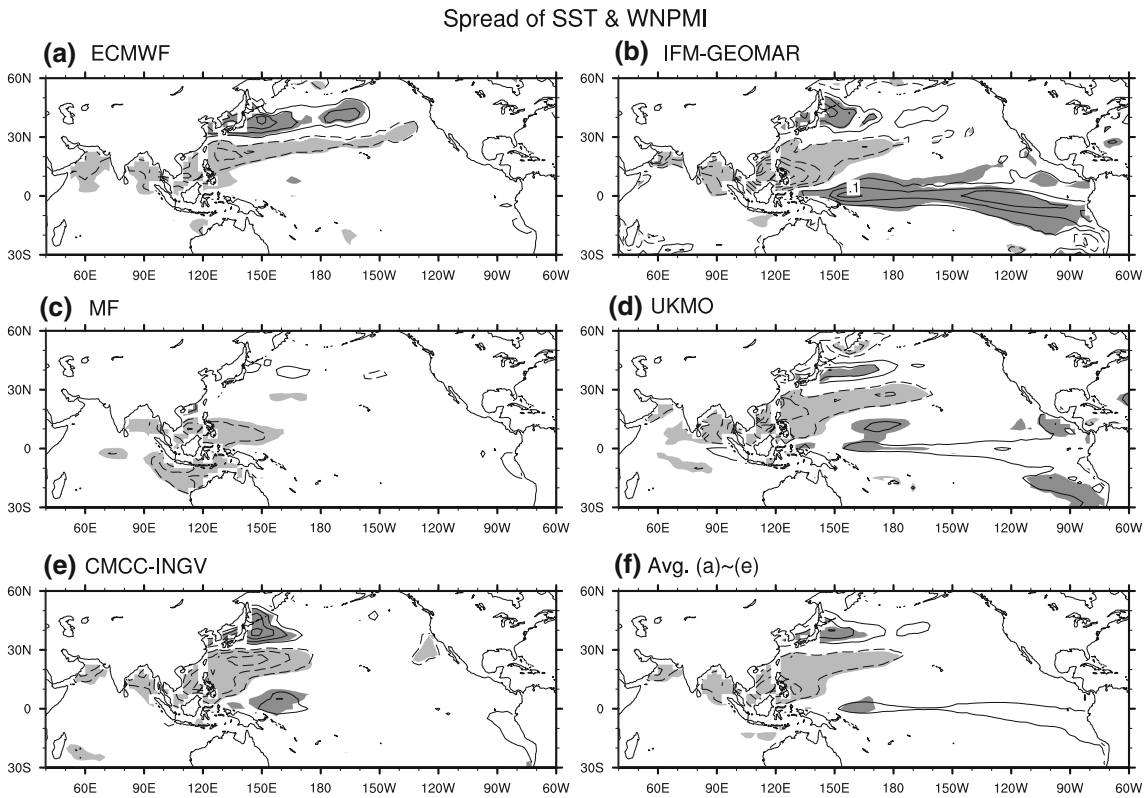

Fig. 12 Same as Fig. 11, but for the regression of the SST anomalies and the interval is 0.05°C

spread of the WNPMI resemble well the observed anomalies in the extratropical WNP.

The precipitation anomalies associated with the prediction spread of the WNPMI (Fig. 13) show significantly more precipitation in the Philippine Sea and less precipitation over the East Asian rainy band and the Indian Ocean. For most models, these spread-related precipitation anomalies show a spatial pattern similar to the precipitation anomalies associated with the interannual WNPMI variability in observations (Fig. 9e). In the MF model, the location of the positive precipitation anomaly over the WNP is shifted equatorward in comparison with that in other models. This equatorward shifted precipitation anomaly may lead to weaker easterly anomaly in the subtropics and westerly anomaly in the middle latitudes shown in Fig. 11c, since the major extent of the positive precipitation anomaly in the WNP is located over the region of climatological easterly flow in the middle and upper troposphere.

The SST anomalies in the extratropics associated with the prediction spread of the WNPMI are consistent with oceanic responses to the atmospheric circulation anomalies above. The 850-hPa wind anomalies shown in Fig. 11 are quite similar with the 10 m wind anomalies associated with the WNPMI prediction spread (not shown), which drive the ocean through wind stress. Thus, the cyclonic circulation anomaly over the subtropical WNP induces upwelling and resultant colder SSTs through the Ekman pumping, while the anticyclonic circulation anomaly over the mid-latitude WNP induces warmer SSTs. In addition, the negative SST anomaly over the north Indian Ocean (Fig. 12) might be caused by the westerly anomaly (Fig. 11), which superposes on the climatological westerly, increases the total wind speed and thus leads to a local evaporative cooling. The SST anomalies in the tropics and subtropics, in turn, can favor the maintenance of the lower-tropospheric circulation anomalies. The negative SST anomaly in the Indian Ocean (Fig. 12) favors less precipitation (Fig. 13), which induces a westerly anomaly in the tropical western

Table 4 Averaged SST anomalies of observation, MME and spread of the integrations regressed onto the normalized WNPMI over the north Indian Ocean (0–25°N, 40°–100°E) (left row), the WNP (10°–30°N, 110°–150°E) (middle row) and the mid-latitude WNP (30°–50°N, 120°–160°E) (right row)

	North Indian Ocean	WNP	Mid-latitude WNP
OBS	−0.098	−0.097	0.110
MME	−0.124	−0.092	0.016
Spread	−0.028	−0.076	0.062

Unit: °C

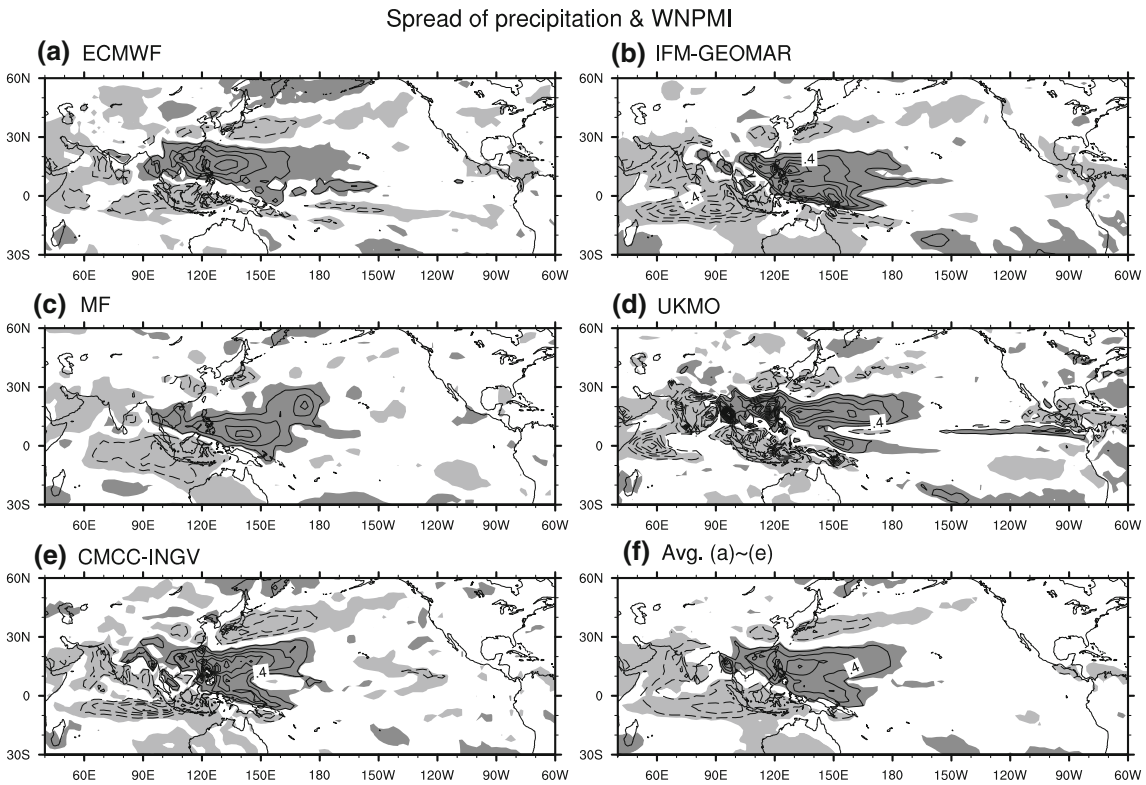

Fig. 13 Same as Fig. 11, but for the regression of the precipitation anomalies and the interval is 0.2 mm day^{-1}

Pacific (Fig. 11). This westerly anomaly can enhance the moisture transport into the tropical WNP and resultant more precipitation (Fig. 13), which induces a cyclonic anomaly over the WNP through the Gill-pattern response.

The above discussions suggest that the SST, precipitation, and lower-tropospheric circulation anomalies related to the prediction spread of the WNPMI are also coupled over the WNP. In addition, there is a positive SST anomaly locating in the subtropical central North Pacific in the IFM-GEOMAR and UKMO (Fig. 12). This positive anomaly and the negative SST anomaly in the subtropical WNP suggest the local air–sea interaction plays an important role in the prediction spread. The positive SST anomaly in the equatorial Pacific shows that the remote forcing from the equatorial Pacific to some extent contributes to the spread of the WNP prediction for the model IFM-GEOMAR.

Comparing anomalies associated with the interannual variation of the WNPMI in observations and in the MME prediction (Fig. 9), the summer anomalies associated with the prediction spread of the WNPMI show a similar spatial pattern. The negative SST anomaly in the north Indian Ocean, the positive precipitation anomalies in the Philippine Sea and the PJ pattern or EAP pattern shown by the anomalies over the WNP (Nitta 1987; Huang and Sun 1992) are noticed in both the prediction spread and MME prediction. However, there are still significant differences among these anomalies. Firstly, the anomalous westerly associated with the spread around the Philippines is slightly weaker and the easterly along 30°N over the mid-latitude WNP is slightly stronger in the averaged results (Fig. 11f) than the MME prediction (Fig. 9b). The westerly over the mid-latitude WNP associated with the prediction spread, which doesn't appear in the MME prediction, resembles better that in observations. Secondly, the SST anomalies associated with the prediction spread are weaker in the north Indian Ocean and subtropical WNP, but stronger in the mid-latitude WNP (Table 4). This implies that the SST anomaly over the north Indian Ocean might not be the primary reason for the spread of the WNPMI prediction. This is different from the MME prediction, in which the cyclonic anomaly over the subtropical WNP results, at least partially, from the zonal gradient of SST anomalies between the tropical Indian Ocean and Pacific (Terao and Kubota 2005). Thirdly, the positive precipitation anomalies associated with the prediction spread (Fig. 13) are about half of those associated with the MME prediction (Fig. 9f) over the subtropical WNP. In summary, the summer anomalies associated with the prediction spread are weaker than the MME prediction over the subtropical WNP. The anomalies in the MME prediction resemble well those in observations in the tropics, while the anomalies for the spread resemble well the observed anomalies in the extratropical WNP.

The local relationships among circulation, SST and precipitation anomalies associated with the prediction

spread of the WNPMI are similar to those associated with the interannual variation of the WNPMI in the MME prediction. As described before, the positive precipitation anomalies around the Philippines (Fig. 13) and the negative SST anomalies over the Indian Ocean (Fig. 12) favor the maintenance of the cyclonic anomalies over the subtropical WNP (Fig. 11). In addition, the anomalous cold SST over the subtropical WNP and warm SST over the subtropical central North Pacific, though weaker than those in the MME prediction, also play an important role in the maintenance of the WNP cyclone through local air–sea interaction (Wang et al. 2000). On the other hand, the anticyclonic circulation anomalies associated with the prediction spread are more significant over the mid-latitude WNP than those associated with the MME prediction and favor the SST warming through the Ekman pumping.

In summary, the WNP summer anomalies related to the prediction spread of the WNPMI demonstrate a spatial pattern similar to those related to the interannual variability of the WNPMI in the MME prediction. However, the magnitudes of these anomalies are different. The anomalies associated with the prediction spread of the WNPMI are relatively weaker over the tropics and resemble better those in observations over the mid-latitude WNP compared with the anomalies associated with the interannual variation of the WNPMI in the MME prediction. The similarity of SST and circulations anomalies associated with the prediction spread in the Indian Ocean and the subtropical central North Pacific to those associated with the interannual variability in observations and in MME implies that the local coupled air–sea interactions plays an important role in the prediction spread. In addition, large SST and circulation anomalies over the extratropical WNP associated with the prediction spread suggest that the atmospheric variability in extratropics might also play a role in the prediction spread over the WNP and East Asia.

5 Summary

In this study, we used five state-of-the-art atmosphere-ocean coupled circulation models from ENSEMBLES to assess the predictability of the summer climate over the WNP with the 1-month lead predictions and investigated the source and limitation of the predictability. A series of skills, including temporal correlation coefficient and two typical precipitation and lower-tropospheric circulation indices, were evaluated during a 46-year period from 1960 to 2005. As each model consists of 9 initial-condition members, the spatial distribution of the lower-tropospheric circulation, SST and precipitation anomalies related to the prediction spread of the WNPMI were also examined.

Spatial distribution of prediction skills from the models shows that current CGCMs have a good capability in reproducing the interannual variation of the WNP summer climate. High prediction skill regions of precipitation stretch from the west Pacific warm pool to the east of Taiwan and cover the majority regions of the Maritime Continent and the east of the Philippines. Additionally, high skill regions of the lower-tropospheric winds cover almost the whole WNP. Interannual variation of SST anomalies over the WNP is also well captured by ENSEMBLES models.

The models also exhibit considerable good performances on the indices which can well represent the variation of precipitation and lower-tropospheric circulation over the WNP. The correlation coefficient of the WNP precipitation index between observations and the MME prediction reaches 0.66 during 1979–2005. For the lower-tropospheric circulation anomalies over the WNP, the interannual variation of the WNPMI is well predicted by ENSEMBLES, with the correlation coefficient of 0.68 in MME during the 46-year period. Standard deviations of the WNP summer precipitation anomalies and the WNPMI produced by the models are also close to the observed ones.

The tropical summer anomalies associated with the interannual variation of the WNP summer climate are well described by the models. The models well capture precipitation anomalies over the Philippine Sea, and SST anomalies over the north Indian Ocean, around the Philippines and the equatorial central Pacific Ocean, which are closely related to the lower-tropospheric anticyclonic/cyclonic anomaly over the WNP in observations. These suggest that the tropical atmosphere–ocean interactions over these regions might be the primary sources of the predictability of the WNP summer climate and imply that continuing improvement in the representation of the air–sea interaction over these regions in CGCMs is a key for long-lead seasonal forecast over the WNP.

The lower-tropospheric circulation, SST and precipitation anomalies related to the spread of the WNPMI exhibit a meridional teleconnection pattern over the tropical and extratropical WNP. They are associated with a significant anomalous cyclone and anticyclone in the subtropical and mid-latitude WNP, respectively. Spatial distribution of SST anomalies related to the spread is a seesaw pattern with cold anomalies over the subtropical WNP and warm anomalies in the mid-latitude WNP, as well as weak SST anomalies over the north Indian Ocean and the tropical western Pacific. Spread of the precipitation anomalies is mainly associated with positive anomalies over the subtropical WNP and negative anomalies in the Indian Ocean and along the East Asian rainy band. In many aspects, the summer anomalies related to the WNPMI prediction spread show a spatial distribution similar to those related to the

interannual variation of the WNPMI in observations and in the MME prediction. But comparing with the MME prediction, the anomalies associated with the prediction spread are relatively weaker over the tropical and subtropical WNP and resemble better with observations over the mid-latitude WNP. These results suggest that the WNP prediction spread is mainly attributable to the internal dynamics in air–sea interaction over the WNP and Indian Ocean. The large circulation and SST anomalies over the extratropical and subtropical WNP in the prediction spread suggest that the extratropical variability might also play a role in the prediction spread over the WNP and East Asia. The results from this study imply that continuing improvement of the air–sea interaction over the tropical oceans in CGCMs and improving atmosphere and land surface initialization will be crucial for the improvement of the long-lead prediction of the summer climates over the WNP and East Asia.

Acknowledgments We thank two anonymous reviewers for their valuable comments. This work was supported by the National Natural Science Foundation of China (Grant Nos. 40810059005, 40821092 and 40975046). BD is supported by the UK National Centre for Atmospheric Science-Climate (NCAS-Climate) at the University of Reading.

References

Adler RF, Huffman GJ, Chang A, Ferraro R, Xie P, Janowiak J, Rudolf B, Schneider U, Curtis S, Bolvin D, Gruber A, Susskind J, Arkin P (2003) The Version-2 Global Precipitation Climatology Project (GPCP) monthly precipitation analysis (1979—present). J Hydrometeor 4:1147–1167

Chou C, Tu JY, Yu JY (2003) Interannual variability of the western North Pacific summer monsoon: differences between ENSO and non-ENSO years. J Clim 16:2275–2287

Chowdary JS, Xie S-P, Luo J–J, Hafner J, Behera S, Masumoto Y, Yamagata T (2009) Predictability of Northwest Pacific climate during summer and the role of the tropical Indian Ocean. Clim Dyn 36:607–621. doi:10.1007/s00382-009-0686-5

Chowdary J, Xie S-P, Lee J-Y, Kosaka Y, Wang B (2010) Predictability of summer Northwest Pacific climate in eleven coupled model hindcasts: local and remote forcing. J Geophys Res 115:D22121. doi:10.1029/2010JD014595

Doblas-Reyes FJ, Weisheimer A, Déqué M, Keenlyside N, McVean M, Murphy J, Rogel P, Smith D, Palmer TN (2009) Addressing model uncertainty in seasonal and annual dynamical ensemble forecasts. Q J R Meteorol Soc 135:1538–1559. doi:10.1002/qj.464

Doblas-Reyes FJ, Weisheimer A, Palmer TN, Murphy JM, Smith D (2010) Forecast quality assessment of the ENSEMBLES seasonal-to-decadal Stream 2 hindcasts. ECMWF Technical Memorandum No. 621, ECMWF, Reading, UK, 45 p

Huang G (2004) An index measuring the interannual variation of the East Asian summer monsoon—the EAP index. Adv Atmos Sci 21:41–52

Huang R, Sun F (1992) Impacts of the tropical western Pacific on the East Asian summer monsoon. J Meteor Soc Jpn 70:243–256

Huang G, Hu K, Xie S-P (2010) Strengthening of tropical Indian Ocean teleconnection to the Northwest Pacific since the mid-1970s: an atmospheric GCM study. J Clim 23:5294–5304

Kalnay E, Kanamitsu M, Kistler R, Collins W, Deaven D, Gandin L, Iredell M, Saha S, White G, Woollen J (1996) The NCEP/NCAR 40-year reanalysis project. Bull Am Meteorol Soc 77:437–471

Kobayashi C, Maeda S, Ito A, Matsushita Y, Takano K (2005) Relation between SSTs and predicability of seasonal mean precipitation over the western tropical Pacific. J Meteor Soc Jpn 83:919–929

Lau K, Kim K, Yang S (2000) Dynamical and boundary forcing characteristics of regional components of the Asian summer monsoon. J Clim 13:2461–2482

Lee J-Y, Wang B, Kang I-S, Shukla J et al (2010) How are seasonal prediction skills related to models' performance on mean state and annual cycle? Clim Dyn 35:267–283. doi:10.1007/s00382-010-00857-4

Lee S-S, Lee J-Y, Ha K-J, Wang B, Schemm J (2011) Deficiencies and possibilities for long-lead coupled climate prediction of the western North Pacific-East Asian summer monsoon. Clim Dyn 36:1173–1188. doi:10.1007/s00382-010-0832-0

Li S, Lu J, Huang G, Hu K (2008) Tropical Indian Ocean basin warming and East Asian summer monsoon: a multiple AGCM study. J Clim 21:6080–6088

Liang J, Yang S, Hu ZZ, Huang B, Kumar A, Zhang Z (2009) Predictable patterns of the Asian and Indo-Pacific summer precipitation in the NCEP CFS. Clim Dyn 32:989–1001. doi:10.1007/s00382-008-0420-8

Lu R (2001) Interannual variability of the summertime North Pacific subtropical high and its relation to atmospheric convection over the warm pool. J Meteor Soc Jpn 79:771–783

Lu R (2002) Precursory SST anomalies associated with the convection over the western Pacific warm pool. Chin Sci Bull 47:696–699

Lu R, Dong B (2001) Westward extension of North Pacific subtropical high in summer. J Meteor Soc Jpn 79:1229–1241

Lu R, Lin Z (2009) Role of subtropical precipitation anomalies in maintaining the summertime meridional teleconnection over the western North Pacific and East Asia. J Clim 22:2058–2072

Lu R, Li Y, Dong B (2006) External and internal summer atmospheric variability in the western North Pacific and East Asia. J Meteor Soc Jpn 84:447–462

Nitta T (1987) Convective activities in the tropical western Pacific and their impact on the Northern Hemisphere summer circulation. J Meteor Soc Jpn 65:373–390

Palmer TN, Alessandri A, Andersen U, Cantelaube P et al (2004) Development of a European multi-model ensemble system for seasonal to inter-annual prediction (DEMETER). Bull Am Meteorol Soc 85:853–872. doi:10.1175/BAMS-85-6-853

Rajeevan M, Unnikrishnan CK, Preethi B (2011) Evaluation of the ENSEMBLES multi-model seasonal forecasts of Indian summer monsoon variability. Clim Dyn. doi:10.1007/s00382-011-1061-x

Rodwell MJ, Hoskins BJ (2001) Subtropical anticyclones and summer monsoons. J Clim 14:3192–3211

Smith TM, Reynolds RW (2004) Improved extended reconstruction of SST (1854–1997). J Clim 17:2466–2477

Terao T, Kubota T (2005) East-west SST contrast over the tropical oceans and the post El Niño western North Pacific summer monsoon. Geophys Res Lett 32:L15706. doi:10.1029/2005GL023010

van der Linden P, Mitchell JFB (eds) (2009) ENSEMBLES: climate change and its impact: summary of research and results from ENSEMBLES project. Met Office Hadley Centre, FitzRoy Road, Exeter EX1 3PB, UK, 160 p

Wang B, Fan Z (1999) Choice of South Asian summer monsoon indices. Bul Am Meteorol Soc 80:629–638

Wang H, Fan K (2009) A new scheme for improving the seasonal prediction of summer precipitation anomalies. Weather Forecast 24:548–554. doi:10.1175/2008WAF2222171.1

Wang B, Wu R, Fu X (2000) Pacific-East Asian teleconnection: how does ENSO affect East Asian climate? J Clim 13:1517–1536

Wang B, Wu R, Lau KM (2001) Interannual variability of the Asian summer monsoon: contrasts between the Indian and the western North Pacific–East Asian monsoons. J Clim 14:4073–4090

Wang B, Kang I-S, Lee J-Y (2004) Ensemble simulations of Asian-Australian monsoon variability by 11 AGCMs. J Clim 17: 803–818

Wang B, Ding Q, Fu X, Kang IS, Jin K, Shukla J, Doblas-Reyes FJ (2005) Fundamental challenge in simulation and prediction of summer monsoon rainfall. Geophys Res Lett 32:L15711. doi:10.1029/2005GL022734

Wang B, Lee JY, Kang IS, Shukla J, Kug JS, Kumar A, Schemm J, Luo J–J, Yamagata T, Park CK (2008) How accurately do coupled climate models predict the leading modes of Asian-Australian monsoon interannual variability? Clim Dyn 30:605–619. doi:10.1007/s00382-007-0310-5

Wang B, Lee JY, Kang IS et al (2009) Advance and prospectus of seasonal prediction: assessment of the APCC/CliPAS 14-model ensemble retrospective seasonal prediction (1980–2004). Clim Dyn 33:93–117. doi:10.1007/s00382-008-0460-0

Wu Z, Li J (2008) Prediction of the Asian-Australian monsoon interannual variations with the grid-point atmospheric model of IAP LASG (GAMIL). Adv Atmos Sci 25:387–394

Wu R, Kirtman BP, Pegion K (2006) Local air-sea relationship in observations and model simulations. J Clim 19:4914–4932

Wu B, Zhou T, Li T (2009) Contrast of rainfall–SST relationships in the Western North Pacific between the ENSO-developing and ENSO-decaying summers. J Clim 22:4398–4405

Xie S-P, Hu K, Hafner J, Tokinaga H, Du Y, Huang G, Sampe T (2009) Indian Ocean capacitor effect on Indo-Western Pacific climate during the summer following El Niño. J Clim 22:730–747

Xie S-P, Du Y, Huang G, Zheng X-T, Tokinaga H, Hu K, Liu Q (2010) Decadal Shift in El Niño Influences on Indo–Western Pacific and East Asian Climate in the 1970s. J Clim 23: 3352–3368. doi:10.1175/2010JCLI3429.1

Yan L, Wang P, Yu Y, Li L, Wang B (2010) Potential predictability of sea surface temperature in a coupled ocean-atmosphere GCM. Adv Atmos Sci 27:921–936

Yang J, Liu Q, Xie S-P, Liu Z, Wu L (2007) Impact of the Indian Ocean SST basin mode on the Asian summer monsoon. Geophys Res Lett 34:L02708. doi:10.1029/2006GL028571

Yang S, Zhang Z, Kousky VE, Higgins RW, Yoo SH, Liang J, Fan Y (2008) Simulations and seasonal prediction of the Asian summer monsoon in the NCEP Climate Forecast System. J Clim 21: 3755–3775

Zhou T, Wu B, Wang B (2009) How well do atmospheric general circulation models capture the leading modes of the interannual variability of the Asian-Australian monsoon? J Clim 22: 1159–1173